UNIVERSITY OF NAPLES FEDERICO II

PH.D. PROGRAM IN

CLINICAL AND EXPERIMENTAL MEDICINE

CURRICULUM IN CARDIOVASCULAR AND GERONTOLOGICAL SCIENCES

XXX Cycle
(Years 2014-2017)

Chairman: Prof. Gianni Marone

PH.D. THESIS

UNFOLDED PROTEIN RESPONSE SIGNALING PATHWAY REGULATES CARDIAC FUNCTION IN HEART FAILURE WITH PRESERVED EJECTION FRACTION

TUTOR
Chiar.mo
Prof. Giovanni Esposito

PH.D. STUDENT
Dr. Gabriele Giacomo Schiattarella

Table of contents

Abstract

Heart failure with preserved ejection fraction (HFpEF) is a clinical syndrome effecting more than 3 million people in the United States alone. HFpEF patients have a 5-year survival rate of less than 50% with no change in prognosis over the last 30 years. The lack of clinical treatments point to an urgent need for mechanistic studies of HFpEF pathogenesis. The cardiac remodeling and dysfunction in HFpEF is driven by comorbidities such as obesity, diabetes, arterial hypertension and endothelial dysfunction which lead to systemic inflammation. Here we report that, in mice, simultaneous metabolic and hypertensive stress, through the combination of high fat diet (HFD) and constitutive nitric oxide (NO) synthase inhibition by administration of $N^{[w]}$-nitro-l-arginine methyl ester (L-NAME) recapitulates systemic and cardiovascular alterations of human HFpEF. The heart failure phenotype was only observed under combined treatment with HFD and L-NAME and was associated with molecular changes within the cardiomyocytes. Specifically, the spliced form of X-box binding protein 1 (Xbp1s), a downstream effector of the unfolded protein response (UPR), exhibited a significant reduction in the HFpEF model hearts and cardiomyocytes. This decrease in Xbp1s was also observed in human HFpEF hearts. Reduction in Xbp1s was caused by increased inducible NO synthase (iNOS) activity and S-nitrosylation of IRE1α, which ultimately led to a defect in XBP1 splicing activity. Importantly, cardiomyocyte-specific inducible overexpression of Xbp1s partially ameliorated diastolic dysfunction, exercise intolerance and pulmonary congestion in HFpEF mice. We have developed a novel preclinical model of HFpEF, unveiling iNOS-driven dysregulation of Xbp1s as a crucial mechanism of cardiomyocyte dysfunction. These results demonstrate the essential role of protein homeostasis dysregulation in HFpEF cardiomyocytes and suggest that inhibiting iNOS activity may be a viable therapeutic strategy in this condition.

Main text

HFpEF is a burgeoning public health problem, representing approximately 50% of HF hospital admissions[1]. The complex clinical phenotype that characterizes this syndrome stems from the presence of multiple comorbidities, such as obesity, hypertension, diabetes mellitus, and endothelial dysfunction[2]. Recent evidence suggests that systemic inflammation, oxidative stress and imbalance in NO levels are crucial for the development of clinical HFpEF[3]. The absence of truly informative preclinical models of HFpEF has led to the lack of knowledge of the basic pathophysiological mechanisms of this syndrome and has obviated the emergence of effective therapies[2,4,5].

The prevalence of the dual comorbidities of obesity and hypertension in HFpEF patients led us to develop our "two-hit" hypothesis. We postulated that the combination of metabolic stress and hypertensive stress in the animals may create the conditions in which the pathogenesis and clinical outcomes of human HFpEF could be recapitulated. C57BL/6 wild-type mice were broken into four groups and fed with 1) high-fat diet (HFD; 60% fat from lard); 2) $N^{[w]}$-nitro-l-arginine methyl ester (L-NAME; 0.5 g/L in drinking water), an inhibitor of nitric oxide (NO) constitutive synthases; 3) a combination of both treatments (HFD+L-NAME) or 4) standard (CHOW) diet for 5/15 weeks (**Fig. 1a**). We chose to treat mice with L-NAME, which is widely used to induce experimental hypertension in laboratory animals[6,7], because multiple lines of evidence suggest that NO dysregulation plays an important role in the pathophysiology of human HFpEF[3,8,9]. Endothelial dysfunction-induced hypertension, together with the multiple features of metabolic syndrome induced by HFD, represent our hypothesized "two-hit" mechanism underlying the natural history of HFpEF.

Mice within all four groups were treated for 5 and 15 weeks and as expected, mice in the HFD groups showed an increase in body weight (BW) compared to mice fed a regular CHOW diet (**Extended data fig 1a**). No effect on BW was observed after administration of L-NAME

in both CHOW and HFD mice (L-NAME and HFD+L-NAME) (**Extended Data Fig.1a**). To evaluate glucose tolerance, intraperitoneal glucose tolerance tests (ipGTT) was performed. Consistently, both HFD and HFD+L-NAME mice exhibit glucose intolerance as evidenced by the persistence of high blood glucose levels compared to CHOW and L-NAME groups (**Extended Data Fig.1b-e**). As expected, L-NAME-treated mice, in both the CHOW or HFD regimen, exhibit a significant increase in systolic and diastolic blood pressure (SBP and DBP, respectively) that stabilized within 4-5 weeks and did not further increase in the 15-week time period (**Extended Data Fig.1f,g**). Thus we established a condition whereby cardiac function could be assessed under metabolic dysfunction and hypertensive stress, individually and in combination.

Normal left ventricular (LV) EF and evidence of diastolic LV dysfunction represent two hallmarks of clinical HFpEF. To explore cardiac function in the different cohorts of mice, we evaluated both systolic and diastolic LV performance by non-invasive echocardiography. Cardiac function was assessed after both 5 weeks and 15 weeks of treatment (**Fig. 1a**). Systolic function as measured by EF% was normal after 15 week-treatment, in all the groups (**Fig. 1b,c and Extended Data Table 1**) as well as at 5-week time point (**Extended Data Fig. 2a and Extended Data Table 1**).

While human HFpEF patients have conserved EF%, many demonstrate impaired systolic function by measurements of longitudinal strain (LS) that correlates with diminished outcomes[10]. Interestingly, a more in deep evaluation of systolic function by speckle-tracking echocardiography reveals significant alterations of LV global LS (GLS) only in HFD+L-NAME mice at both time points evaluated (**Fig.1d and Extended Data Fig. 2b**) demonstrating impaired systolic function despite preserved EF in these cohorts of mice as well.

However, differential degrees of diastolic dysfunction were found in mice treated with HFD or L-NAME alone, with HFD-treated mice for 15 weeks showing a decrease in the early (E)

wave and increased atrial (A) wave of mitral pulse doppler (E/A) indicative of impaired relaxation found in early stage of diastolic dysfunction (**Fig.1e,f**) which was not yet detectable in the 5-week cohort (**Extended Data Fig. 2c**). In contrast, mice with the L-NAME treatment alone exhibit a restrictive pattern of diastolic dysfunction that is exacerbated by the HFD treatment at both time points (**Fig.1e,f and Extended Data Fig. 2c**). Indeed, the combinatory diet treated animals (HFD + L-NAME) display signs of significantly increased LV filling pressure as evidenced by increased E/A (**Fig.1e,f and Extended Data Fig. 2c**) as well as the increased ratio between E' wave and the E' wave on mitral tissue doppler (E/E'; **Fig.1e,g and Extended Data Fig. 2d**). Importantly, the highest degree of diastolic dysfunction in 15-week-treated HFD+L-NAME mice was also confirmed by invasive hemodynamics data using pressure-volume (PV) loop analysis (**Extended Data Table 1**). These data indicate that a combination of HFD and L-NAME treatment can act in concert to produce a condition of diastolic dysfunction with preserved ejection fraction significantly worse than either treatment alone.

A key component to a successful model of HFpEF is evidence of HF. One marker of HF is reduced exercise tolerance, which correlates with symptoms in clinical studies[11]. To investigate the tolerance to physical exercise in our model of HFpEF, we subjected mice from different groups to a treadmill exhaustion test. As expected, weight impacted exercise performance of HFD-treated mice at both 15-week and 5-week time points (**Fig. 1h and Extended Data Fig. 2e**). However, after 15 weeks of the combinatory treatment, HFD+L-NAME mice displayed a significant reduction in running distance compared to all groups including those mice fed only a HFD (**Fig.1h**). Furthermore, while hearts from all three treated groups exhibit cardiac hypertrophy, as shown by the increase in heart weight/tibia length ratio (HW/TL) (**Fig. 1i and Extended Data Fig. 2f**), this response is greatest in the HFD+L-NAME mice after 15 weeks of treatment (**Fig.1i**) More importantly, only the HFD+L-NAME mice exhibit signs of HF, as

shown by robust increase in the ratio of wet:dry lung weight (LW) (**Fig.1j and Extended Data Fig. 2g**), a marker of pulmonary congestion and a preclinical surrogate for HF. Cardiac structure alterations were also found. Indeed, histological analysis of 5 week-treated hearts, revealed increased heart mass, cardiomyocyte hypertrophy and increased fibrosis in mice treated with L-NAME or the combination of HFD+L-NAME (**Extended Data Fig. 3a-c**). Collectively these results demonstrated that the HFD+L-NAME mice recapitulate the systemic and cardiac alterations of HFpEF patients including diastolic dysfunction and HF.

Microvascular alterations and increased vascular stiffness are also recognized in clinical HFpEF[12]. Mice subjected to as little as 5 week-chronic L-NAME treatment exhibit high aortic stiffness as shown by a significant increase in pulse wave velocity (PWV) across the arterial system (**Extended Data Fig.4a**). Subsequently, in order to explore the presence of coronary dysfunction in mice subjected to the different treatments, we measured coronary flow reserve (CFR) using short term exposure of high isoflurane (Iso) to induce hyperemic coronary blood flow. Interestingly in both L-NAME and HFD+L-NAME mice, the coronary vasodilatatory response induced by Iso was significantly blunted, with parallel reduction of CFR (**Extended Data Fig. 4b,c**). Finally, myocardial capillary density was also significantly reduced in L-NAME-treated mice (**Extended Data Fig. 4d,e**). Although the vascular alterations occurred in all L-NAME treated groups, the addition of increased diastolic dysfunction and the HF symptoms in the HFD + L-NAME group further supports this treatment as a model of HFpEF.

Although HFpEF is known to be a systemic disease involving complex pathophysiological interactions between different cell types, tissues and organs, alterations in cardiomyocyte contraction and relaxation represent to date a recognized common background[13,14]. Adult mouse ventricular myocytes (AMVMs) were isolated from hearts of different experimental groups after 5 weeks of dietary regimen in order to investigate the presence of cardiomyocyte dysfunction. AMVMs were externally paced and rates of sarcomeres shortening and

relengthening were measured after electrical stimulation. Interestingly, although no differences were observed in baseline sarcomeric length (**Extended Data Fig.5a**) and in time to peak velocity (**Extended Data Fig.5b**) among the four groups, AMVMs isolated from HFD+L-NAME mice exhibit a significant reduction in contraction and impaired relaxation (**Extended Data Fig.5c-f**) compared to AMVMs isolated from other experimental groups. These data confirmed that the alterations in cardiac mechanics observed in our HFpEF model can be recapitulated in isolated AMVMs

Our evidence thus far suggested that, functionally and structurally, HFD+L-NAME treatment results in distinct functional and physical changes in the heart compared to either treatment alone, mirrored many of the clinical symptoms of human HFpEF. We next looked for molecular differences in cardiomyocytes between these groups that might provide insight to the pathological progression of this syndrome. The unfolded protein response (UPR) represents a crucial adaptive response system able to mitigates stress under many conditions that interfere with protein quality control[15]. Recently, accumulation of misfolded proteins has been recognized in clinical HFpEF, posing the attention on protein handling dysregulation also in this syndrome[16]. Regulators of protein quality control in HFpEF are currently unknown. Although the activation of all three branches of UPR – inositol-requiring protein 1α(IRE1α), protein kinase RNA-like ER kinase (PERK), and activating transcription factor 6 (ATF6) transducers – happens in many diseases, disproportional activation of single branches it has also been reported[17,18]. In this context, IRE1α plays an important role in maintaining endoplasmic reticulum (ER) function through initiating unconventional splicing of the mRNA encoding X-box–binding protein 1 (Xbp1) to generate spliced X-box binding protein 1 (Xbp1s), a powerful transcription factor involved in many fundamental cellular functions[15]. We recently discovered the cardioprotective role of Xbp1s overexpression during cardiac ischemia/reperfusion injury[19] and we hypothesized that activation of the UPR can trigger beneficial effects on cardiac

remodeling also during the development of HFpEF. Therefore, we first analyzed the mRNA expression levels of the most important UPR markers in hearts of different experimental groups after 5 weeks of dietary regimen. As expected, we found a strong activation of UPR sensors and effectors in HFD and L-NAME hearts, but surprisingly a significant reduction below baseline in expression levels of Xbp1s, BIP, CHOP was found in HFD+L-NAME mouse hearts (**Fig. 2a**). Importantly, we confirmed Xbp1s and other markers inactivation also in AMVMs isolated from HFD+L-NAME mice at both mRNA and protein level (**Fig. 2b,c**). These findings show a clear molecular difference in the cardiomyocytes of HFD+L-NAME treated animals that correlates with the emergence of HF.

We next turned to endomyocardial biopsies of control and failing human hearts to see if the molecular changes we observed also occurred. Strikingly, Xbp1s mRNA levels was also found downregulated in human HFpEF myocardium but not in samples from patients with HF with reduced ejection fraction (HFrEF) (**Fig. 2f and Extended Data Table 2**). These data confirm that the Xbp1s downregulation observed in our animal model also occurs in the context of human HFpEF.

Our data showed that the down-regulation of Xbp1s correlated with the development of HFpEF in our animal model. To examine more directly whether a decrease in this transcription factor could be complicit in the pathophysiology of HFpEF, we took advantage of a cardiomyocyte-specific Tet-off Xbp1s overexpression transgenic mouse line (TG)[19]. Xbp1s is expressed only in cardiomyocytes and suppressed in the presence of doxycycline (Doxy). Littermate control (CTR) and Xbp1s transgenic animals (TG) were treated with either normal CHOW or HFD+L-NAME with the presence of Doxy in the drinking water (**Fig. 3a**). Serial echoes, both before treatment and 5 weeks after treatment, were done to confirm the diastolic dysfunction was induced in the HFD+L-NAME groups with conserved LVEF%(**Fig. 3b-d**). Once the phenotype was established Xbp1s expression was induced by removing Doxy for 2

weeks (**Fig. 3a and Extended Data Fig. 7**) and mice were subjected to further functional and molecular analyses. Remarkably, two weeks of Xbp1s expression was sufficient to drive a significant amelioration of the diastolic dysfunction as shown by the reduction of E/A and E/E' ratios compared to CTR (**Fig. 3c, d**) without impacting on LVEF% (**Fig. 3b**). This increase in diastolic performance was associated with a significant increase in exercise tolerance in these animals (**Fig. 3e**) as well as a decrease in pulmonary edema (**Fig. 3f**) and in the mRNA expression of HF-related genes, atrial natriuretic peptide (*nppa*) and brain natriuretic peptide (*nppb*) (**Fig. 3g**). Interestingly, no significant reduction in cardiac hypertrophy was observed after 2 weeks of Xbp1s expression (**Fig. 3h**). Taken together, these data demonstrate that overexpression of Xbp1s in cardiomyocytes is sufficient to ameliorate the diastolic dysfunction and signs of HF observed in HFpEF mice and suggest a model by which decreased Xbp1s levels are a driving force in the development of HFpEF.

As stated before, endothelial dysfunction and dysregulation of NO synthesis represent important components of HFpEF pathophysiology. In fact, L-NAME, which we use as a driver of hypertension, is a potent inhibitor of endothelial NOS (eNOS). However, at the same time L-NAME has also been suggested to be an activator of inducible nitric oxide synthase (iNOS) in cardiovascular system[20]. Similarly, iNOS has been shown to be upregulated in rodent hearts under HFD conditions[21]. We therefore examined whether iNOS levels were altered in our model system. As has been reported, a significant increase of iNOS expression level, was found in the hearts of both HFD and L-NAME treated mice after 5 weeks of dietary regimen, whereas no differences were observed in eNOS expression level (**Fig.4a**). Strikingly, the combination of HFD + L-NAME resulted in a dramatic increase in iNOS levels in the hearts over either single treatment (**Fig.4a**). Isolation of AMVMs from all four groups of these animals confirmed that the changes in iNOS levels were mirrored at the cardiomyocyte level (**Fig.4b**). High levels of NO generate S-nitrosylation of protein's cysteine residues, and can regulate their function[22,23].

Accordingly, we observed a significant increase of total protein nitrosylation in hearts of HFD + L-NAME mice (**Fig.4c,d**).

The observation that levels of iNOS expression was increased in cardiomyocytes from HFD + L-NAME treated mice raised the possibility of a connection between iNOS levels and the decrease in Xbp1s. Prior studies have shown that in the livers of extremely obese mice, iNOS-dependent S-nitrosylation of IRE1α can inhibit its function, resulting in reduction in Xbp1 splicing[21]. In order to examine whether a similar effect can occur in myocytes, recombinant adenovirus driving iNOS expression (AdiNOS) was used in neonatal rat ventricular myocytes (NRVMs). Increasing concentrations of AdiNOS resulted, in a robust increase in iNOS expression whereas control infection with a β-galactosidase adenovirus (AdLacZ) had no effect on iNOS expression (**Extended Data Fig. 6a,b**). iNOS overexpression significantly increases NO production in NRVMs culture media (**Extended Data Fig. 6c**) without significantly impact on cardiomyocyte viability (**Extended Data Fig. 6d**). Importantly, transduction with AdiNOS resulted in a bi-phasic response of Xbp1s mRNA expression levels, with an initial rise and subsequent significant fall below the basal levels (**Extended Data Fig. 6e**). Interestingly this pattern mirrors the correlation between iNOS levels and Xbp1s in the hearts of the four treatment groups. In the HFD+L-NAME hearts, evidence of increased S-nitrosylation of IRE1α (**Fig. 4e,f**) and decreased autophosphorylation of IRE1α (**Fig. 2c**) is observed in support of a mechanism whereby Xbp1s reduction in preclinical HFpEF is attributed to S-nitrosylation of IRE1α.

HFpEF is a lethal disease for which no current therapies have consistently show beneficial effects. Absence of effective etiological therapies in HFpEF is related to the relatively poor knowledge of its fundamental pathophysiological mechanisms, many of them remain hypothetical due to the absence of robust preclinical data. In fact, to date, no reliably predictive,

preclinical models of HFpEF exist as many focus only on single components of the human disease but do not recapitulate its complexity[5,24]. For example, in pressure overload-induced hypertrophy models such as the one realized through transverse aortic constriction (TAC), the presence of HFpEF represents only a transient stage of the natural history of this model, which inexorably progress to HFrEF over time. Given the limitations of current pre-clinical models of HFpEF, we developed a novel murine model of HFpEF in which no apparent reduction in EF has been recognized over a extended period of observation. Indeed, within 5 weeks of treatment the manifestation of the HFpEF phenotype becomes apparent with underlying the fact that the observed cardiovascular phenotype in those mice represents an established disease state.

Moving forward, we extended the knowledge of basic pathophysiological mechanisms of this syndrome. Current thinking identifies inflammation as a major cause of microvascular dysfunction and reduced NO bioavailability in clinical HFpEF. However, although epidemiologic studies have shown increased levels of circulating cytokines[25-27], so far, no mechanistic studies have provided robust evidences of inflammatory involvement in HFpEF pathophysiology. Here we focused on metabolic inflammation (meta-inflammation) and on its master mediator, iNOS, demonstrating the important role of inflammatory-dependent alterations in this syndrome.

Current treatments of HFpEF that have been focused on increasing NO bioavailability have reported neutral[24,28,29] or negative results[30,31]. In our preclinical model of HFpEF we have shown that excessive production of NO, induced by the pro-inflammatory activation of iNOS, affects protein quality control in cardiomyocytes leading to contractile dysfunction. Our results, indeed, give a biological explanation for the failure of NO-inducing approaches as therapeutic options. Therefore, turning the attention to strategies focusing on reducing iNOS activation, as has been done in other disease[32], could represents a valid approach also in HFpEF.

Working from the clinical realities of HFpEF, including multi-organ co-morbidities, we have developed the first murine model of model of HFpEF that recapitulates most of the myriad, features of the clinical syndrome and uncovered a the iNOS-dependent regulation of Xbp1s as a novel pathophysiological mechanism of this syndrome.

Methods

Experimental animals

All experiments involving animals were conform to the Guide for the Care and Use of Laboratory Animals published by the US National Institutes of Health (NIH Publication 8th edition, update 2011), and were approved by the Institutional Animal Care and Use Committee of the University of Texas Southwestern Medical Center. Adult (8-12-week-old), male C57BL/6J mice were used for wild-type (WT) studies. TRE-Xbp1s mouse were crossed with the MHC-tTA mouse model to generate mice with cardiomyocyte-specific deletion of Xbp1s (TG) as previously described[19]. Mice were maintained on a 12-hour light/dark cycle from 6 AM to 6 PM had unrestricted access to food (#2916, Teklad for CHOW groups and D12492, Research Diet Inc. for the HFD groups) and water. $N^{[w]}$-nitro-l-arginine methyl ester (L-NAME; 0.5 g/L, Sigma Adrich) was supplied in drinking water for the indicated periods of time, after adjusting the pH to 7.4.

Conventional echocardiography and Doppler imaging

Transthoracic echocardiography was performed using a VisualSonics Vevo 2100 system equipped with MS400 transducer (Visual Sonics Inc.). Left ventricular (LV) EF and other indexes of systolic function were obtained from short axis M-mode scans at mid ventricular level, as indicated by the presence of papillary muscles, in conscious, gently restrained mice. Apical 4-chamber view was used to obtain diastolic function measurements using pulse wave and tissue Doppler at the level of mitral valve in anesthetized mice. Anesthesia was induced by 5% isoflurane and confirmed by lack of response to firm pressure on one of the hind paws; during echocardiograms acquisition, under body temperature controlled conditions, isofluorane was reduced to 1.0-1.5% and adjusted to maintain heart rate in the range of 415-460 beats per minute monitoring ECG. Parameters include: heart rate (HR), left ventricular end-diastolic

diameter (LVID,d), left ventricular end-systolic diameter (LVID,s), end-diastolic interventricular septal wall thickness (IVS,d), left ventricular end-diastolic posterior wall (LVPW,d), left ventricular fractional shortening (LVFS), left ventricular ejection fraction (LVEF); peak Doppler of blood inflow velocity across mitral during early diastole (E), peak Doppler of blood inflow velocity across mitral during late diastole (A), isovolumic relaxation time (IVRT), peak tissue Doppler of myocardial relaxation velocity at mitral valve annulus during early diastole (E'), early filling deceleration time (DT). At the end of the procedures all mice recovered from anesthesia without difficulties. All parameters were measured at least 3 times and the averages were presented.

Speckle tracking echocardiography and strain analysis

B-mode traces acquired from the parasternal long-axis view were used to calculate global strain for longitudinal dimensions with the VevoStrain software (Visual Sonics Inc.) using a speckle-tracking algorithm. Velocity and displacement were also calculated in both the long- and short-axes. Values generated by strain analysis in longitudinal dimension were negative which illustrates fiber shortening. B-mode images were selected based on the quality of them (high frame rates) and on the ability to visualize both the endocardial and epicardial LV wall borders. Borders of the endocardium and epicardium were traced and semi-automated strain analysis was performed. Average peak global strain values were obtained from six independent anatomical segments of the LV.

Coronary flow reserve

Coronary flow velocity was measured in cine traces of left proximal coronary artery using pulsed-wave Doppler-mode at baseline, and under hyperemic conditions induced by inhalation

of 1.5% and 3.0% isoflurane, respectively. CFR was expressed as the ratio between peak blood flow velocity during hyperemia and peak blood flow velocity at baseline.

Noninvasive blood pressure measurements

Systolic blood pressure was noninvasively measured in conscious mice by tail-cuff method using the CODA instrument (Kent Scientific). Animals were placed in a holder on a temperature-controlled platform (kept at 37 °C), and recordings were performed in steady-state conditions. Blood pressure values were averaged from at least three consecutive measurements.

Pulse wave velocity

Pulse wave velocity (PWV) was noninvasively measured over the entire aorta. Pulsed Doppler images were obtained at the ascending aorta (just cranial to the aortic valve) and the abdominal aorta (just cranial to the iliac bifurcation). Subsequently the distance between both locations was approximated by an external body tape measurement. PWV was calculated as the ratio of X and T (PWV= X/ T), where X is the distance between the due anatomical location where the Doppler signals were recorded and T is the foot-to-foot transit time between averaged waveforms at both locations.

Pressure-volume analysis

Apical approach was used to obtain PV measurements from anesthetized mice using a mouse PV catheter (Milllar instruments). Inferior vena cava was located and occluded during a pause in ventilation to acquire load-independent indexes. Data were analyzed using PV Lab Chart software.

Exercise exhaustion test

After 3 days of acclimatization period on treadmill, exhaustion test was performed in all groups of mice. Animals ran on the treadmill tilted 20° uphill starting at a warm-up speed of 5 m/min for 4 min after which speed was increased to 14m/min for 2 min. Every subsequent 2 min, the speed was increased by 2 m/min until mice were exhausted. Exhaustion was defined as the inability of the animal to return to running within 10 seconds after direct contact with an electric-stimulus grid. Running time was measured and running distance calculated.

Intraperitoneal glucose tolerance test

Intraperitoneal glucose tolerance test (ipGTT) was performed by injection of glucose (2 g/kg in saline) after 6-hour fasting. Tail blood glucose levels [mg/dl] were measured with glucometer before (0 min) and at 15, 30, 45, 60 and 120 min after injection.

Histology

Hearts were fixed in 4% paraformaldehyde (PFA) overnight and paraffin cross-section (5 m) were stained with hematoxylin and eosin, Masson's trichrome. Wheat germ agglutinin (WGA) staining and lectin staining were used to measure cardiomyocyte cross-sectional area and to quantify capillary density respectively. After deparaffinization and antigen retrieval with hot citrate buffer, cardiac slides were incubated with WGA conjugated to Alexa Fluor 488 (50 mg/ml) for one hour at room temperature or with bitoin conjugate lectin from *Griffonia simplicifolia* overnight at 4°C. Cardiomyocyte size and capillary numbers were quantified using Image J software.

Cardiomyocyte isolation

AMVMs were isolated from littermates of different experimental groups. Briefly, hearts were isolated and immediately retrograde perfused with perfusion buffer for 1 min and the switched to a buffer containing liberase-TM (0.025 mg/mL, Roche) and trypsin (0.025%) for 14 min. The left ventricle was dissected and minced in perfusion media supplemented with 10% dialyzed FBS. After filtration, AMVMs were let to sediment by gravity and non-cardiomyocytes were discarded. Calcium reintroduction was done stepwise from 0-1.8 mM in 6 steps. NRVMs were isolated from 1-2 day old Sprague-Dawley rat pups as previously described. Cell preparations contained greater than 95% cardiomyocytes.

Sarcomere length measurements in paced cardiomyocytes

Sarcomere shortening and relaxation was measured in freshly isolated AMVMs using the integrated IonOptix contractility/photometry system. Briefly, AMVMs were electrically stimulated at 0.5 Hz using a field stimulator. Parameters measured include basal sarcomeric length, delta sarcomeric length after contraction, maximum departure/return velocities and time to peak. All measurements were performed at room temperature from 3 different heart preparations per group.

Adenovirus production, purification and infection

Mouse iNOS CDNA was obtained from Addgene (#19295) was subcloned into an adenovirus expression vector using Adeno-X™ Adenoviral System 3 (CMV promoter and Zsgreen1 reporter, Takara) following the manufacturer instructions. Adenoviruses were harvested from culture supernatant and cell lysates, the viral titer was determined, and virus aliquots were store at -80°C. NRVMs were infected with increasing multiplicity of infection

(MOI) of virus and cells were harvested 24-hour post-infection. AdLacz construct contained in the kit was used a control at the same MOI.

RNA Isolation and qPCR

Total RNA was isolated from hearts, AMVMs or NRVMs using TRIzol reagent or Quick-RNA™ MicroPrep kit (Zymo Reaserch). A total of 100-500 ng RNA was used for reverse transcription using iScript reagent (Bio-Rad). qPCR reactions were performed in triplicate with SYBR master mix (Bio-Rad). The 2^{-CT} relative quantification method, using *18S* for normalization, was used to estimate the amount of target mRNA in samples and fold ratios were calculated relative to mRNA expressions levels from control animals. The following PCR primers sequences were used (forward, reverse): *Xbp1s-mouse/rat* (GGTCTGCTGAGTCCGCAGCAGG, GAAAGGGAGGCTGGTAAGGAAC); *BIP-mouse* (CATGGTTCTCACTAAAATGAAAGG, GCTGGTACAGTAACAACTG); *ATF6-mouse* (AGAAAGCCCGCATTCTCCAG, ACTCCCAGAATTCCTACTGATGC); *ATF4-mouse* (ATGGCCGGCTATGGATGAT, CGAAGTCAAACTCTTTCAGATCCATT); *CHOP-mouse* (CTGCCTTTCACCTTGGAGAC, CGTTTCCTGGGGATGAGATA); *NOS2-mouse* (GTTCTCAGCCCAACAATACAAGA, GTGGACGGGTCGATGTCAC); *NOS3-mouse* (TCAGCCATCACAGTGTTCCC, ATAGCCCGCATAGCGTATCAG); *NPPA-mouse* (CTGGGACCCCTCCGATAGAT, TTCGGTACCGGAAGCTGTTG); *NPPB-mouse* (TTTGGGCTGTAACGCACTGAA, TGTGGCAAGTTTGTGCTCCA); *18S-mouse/rat* (AAACGGCTACCACATCCAAG, CCTCCAATGGATCCTCGTTA); *Xbp1s-human* (CTGAGTCCGCAGCAGGTG, GTCCAGAATGCCCAACAGGA); *GAPDH-human* (TCAACGACCACTTTGTCAAGCTCA, GCTGGTGGTCCAGGGGTCTTACT).

Immunoblot analysis

Protein extracts from frozen mouse hearts, AMVMs and NRVMs were obtained by lysis in ice-cold modified RIPA buffer (150 mM NaCl, 50 mM Tris HCL pH 7.4, 1% Triton-X 100, 0.5% sodium deoxycholate, 0.1% SDS, 5 mM EDTA, 2 mM EDTA) containing protease and phosphatase inhibitors. Protein were separated under reducing conditions on SDS-polyacrylamide 4%-20% gradient gels (Bio-Rad) and transferred to nitrocellulose membranes. Proteins were detected with the following primary antibodies: anti-pIRE1α [Ser724] (NB100-2323, Novus Biological); anti-GRP94 (#2104, Cell Signaling); anti-iNOS (#13120, Cell Signaling); anti-GAPDH (10R-G109a, Fitzgerald). Odyssey scanner (LI-COR) was used as a detection system.

Measurement of nitrite and nitrate

The amount of nitrite (NO_2^-) and nitrate (NO_3^-), the breakdown products of NO, were measured in tissue or cell media with the Nitrate/Nitrite colorimetric assay kit (Cayman Chemicals) according to the manufacturer's instructions.

Lactate dehydrogenase (LDH) assay

To evaluate cell survival, LDH assay was performed using the CytoTox96 cytotoxicity kit (Promega) according to the manufacturer's instructions. LDH release was calculated as follow: (medium LDH)/(medium LDH + intracellular LDH).

Determination of S-nitrosylation

Hearts were excised, snap-frozen in liquid nitrogen and stored at -80ºC until homogenization. Tissue was homogenized in immunoprecipitation (IP) buffer (25 mM sodium phosphate pH 7.2, 150 mM, NaCl, 10 % Glycerol, 1 mM EDTA, 1% triton,

protease/phosphatase Inhibitors) supplemented with 0.1 mM neocuproine, using an electric homogenizer on ice. Lysates were spun at 10,000*xg* and supernatants were used for protein determination using BCA method. Free cysteines were blocked at room temperature in HENS buffer (100 mM HEPES (pH 7.0), 1 mM EDTA, 0.1 mM neocuproine, and 2% SDS) using N-Ethylmaleimide (ratio 5 ug NEM per 1 ug protein). Proteins were acetone-precipitated, and pellet washed using acetone:water (4:1). Protein pellet was resuspended in HENS buffer pH8.0 and labeled using 40 mM ascorbic acid and TMT 0.2 mM. Negative control without ascorbic acid and positive control with GSNO 1 mM were included for labeling. Immunoprecipitation was carried out using 500 ug labeled protein and 5 uL IRE1α (Cell Signaling, #3294) and 25 uL Dynabeads Protein G in IP buffer overnight at 4C. Beads were magnetically separated and washed 5 times with IP buffer and then eluted using a 2x Laemmli buffer.

Human myocardial tissue

Human myocardial tissue samples collection was performed under protocols approved by Institutional Review Boards at the Johns Hopkins University (Maryland, USA) and consent for biopsy procedures or use of explanted tissues prospectively obtained in all cases. Explant dilated failing human hearts were procured at the time of orthotopic heart transplantation. Samples were full-thickness biopsies obtained from the free wall of the left ventricle. HFpEF patients were referred for cardiac catheterization and right ventricular endomyocardial biopsy because of clinical suspicion of infiltrative cardiomyopathy. Control samples for these studies were obtained from explanted unused donor hearts.

Statistical analysis

Data is presented as bar graphs or box-and-whisker plots. Bar graph show mean, and the error bars represent S.E.M. Box-and-whisker plots show median, the first and third quartiles,

and minimum and maximum values. All data met assumptions of the statistical test and different groups had similar variance. Differences were analyzed by unpaired Student t test for experiments with 2 groups, or one-way analysis of variance (ANOVA) plus Sidak's *post hoc* test for multiple comparisons or two-way ANOVA plus Tukey–Kramer's *post hoc* test as appropriate in experiments including ≥3 groups. A minimum value of $p<0.05$ was considered statistically significant. All experiments were done with at least three biological replicates. All statistical analyses were conducted using GraphPad Prism software 7.0. Categorical variables in the E**xtended Data Table 2** were compared using chi-square test using SPSS Statistics version 19 (SPSS Inc., Chicago, IL). No statistical analysis was used to predetermine sample size which was chose based on our previous experience. No data were excluded from the analyses. No randomization was used to allocate animals to experimental groups, and investigators were not blinded to group allocation during experiments except for the data included in Extended Data Figure 5.

References

1 Dunlay, S. M., Roger, V. L. & Redfield, M. M. Epidemiology of heart failure with preserved ejection fraction. *Nat Rev Cardiol*, doi:10.1038/nrcardio.2017.65 (2017).

2 Shah, S. J. *et al.* Phenotype-Specific Treatment of Heart Failure With Preserved Ejection Fraction: A Multiorgan Roadmap. *Circulation* **134**, 73-90, doi:10.1161/CIRCULATIONAHA.116.021884 (2016).

3 Chirinos, J. A. & Zamani, P. The Nitrate-Nitrite-NO Pathway and Its Implications for Heart Failure and Preserved Ejection Fraction. *Curr Heart Fail Rep* **13**, 47-59, doi:10.1007/s11897-016-0277-9 (2016).

4 Butler, J., Braunwald, E. & Gheorghiade, M. Recognizing worsening chronic heart failure as an entity and an end point in clinical trials. *JAMA* **312**, 789-790, doi:10.1001/jama.2014.6643 (2014).

5 Roh, J., Houstis, N. & Rosenzweig, A. Why Don't We Have Proven Treatments for HFpEF? *Circ Res* **120**, 1243-1245, doi:10.1161/CIRCRESAHA.116.310119 (2017).

6 Bernatova, I. *et al.* Wine polyphenols improve cardiovascular remodeling and vascular function in NO-deficient hypertension. *Am J Physiol Heart Circ Physiol* **282**, H942-948, doi:10.1152/ajpheart.00724.2001 (2002).

7 Paulis, L. *et al.* Regression of L-NAME-induced hypertension: the role of nitric oxide and endothelium-derived constricting factor. *Hypertens Res* **31**, 793-803, doi:10.1291/hypres.31.793 (2008).

8 Greene, S. J. *et al.* The cGMP signaling pathway as a therapeutic target in heart failure with preserved ejection fraction. *J Am Heart Assoc* **2**, e000536, doi:10.1161/JAHA.113.000536 (2013).

9 van Heerebeek, L. *et al.* Low myocardial protein kinase G activity in heart failure with preserved ejection fraction. *Circulation* **126**, 830-839, doi:10.1161/CIRCULATIONAHA.111.076075 (2012).

10 DeVore, A. D. *et al.* Impaired left ventricular global longitudinal strain in patients with heart failure with preserved ejection fraction: insights from the RELAX trial. *Eur J Heart Fail*, doi:10.1002/ejhf.754 (2017).

11 Haykowsky, M. J., Tomczak, C. R., Scott, J. M., Paterson, D. I. & Kitzman, D. W. Determinants of exercise intolerance in patients with heart failure and reduced or preserved ejection fraction. *J Appl Physiol (1985)* **119**, 739-744, doi:10.1152/japplphysiol.00049.2015 (2015).

12 Franssen, C. *et al.* Myocardial Microvascular Inflammatory Endothelial Activation in Heart Failure With Preserved Ejection Fraction. *JACC Heart Fail* **4**, 312-324, doi:10.1016/j.jchf.2015.10.007 (2016).

13 Primessnig, U. *et al.* Novel pathomechanisms of cardiomyocyte dysfunction in a model of heart failure with preserved ejection fraction. *Eur J Heart Fail* **18**, 987-997, doi:10.1002/ejhf.524 (2016).

14 Methawasin, M. *et al.* Experimentally Increasing the Compliance of Titin Through RNA Binding Motif-20 (RBM20) Inhibition Improves Diastolic Function In a Mouse Model of Heart Failure With Preserved Ejection Fraction. *Circulation* **134**, 1085-1099, doi:10.1161/CIRCULATIONAHA.116.023003 (2016).

15 Wang, Z. V. & Hill, J. A. Protein quality control and metabolism: bidirectional control in the heart. *Cell Metab* **21**, 215-226, doi:10.1016/j.cmet.2015.01.016 (2015).

16 Gonzalez-Lopez, E. *et al.* Wild-type transthyretin amyloidosis as a cause of heart failure with preserved ejection fraction. *Eur Heart J* **36**, 2585-2594, doi:10.1093/eurheartj/ehv338 (2015).

17 Fu, H. Y. *et al.* Chemical Endoplasmic Reticulum Chaperone Alleviates Doxorubicin-Induced Cardiac Dysfunction. *Circ Res* **118**, 798-809, doi:10.1161/CIRCRESAHA.115.307604 (2016).

18 Engin, F. *et al.* Restoration of the unfolded protein response in pancreatic beta cells protects mice against type 1 diabetes. *Sci Transl Med* **5**, 211ra156, doi:10.1126/scitranslmed.3006534 (2013).

19 Wang, Z. V. *et al.* Spliced X-box binding protein 1 couples the unfolded protein response to hexosamine biosynthetic pathway. *Cell* **156**, 1179-1192, doi:10.1016/j.cell.2014.01.014 (2014).

20 Kopincova, J., Puzserova, A. & Bernatova, I. L-NAME in the cardiovascular system - nitric oxide synthase activator? *Pharmacol Rep* **64**, 511-520 (2012).

21 Yang, L. *et al.* METABOLISM. S-Nitrosylation links obesity-associated inflammation to endoplasmic reticulum dysfunction. *Science* **349**, 500-506, doi:10.1126/science.aaa0079 (2015).

22 Martinez-Ruiz, A. *et al.* Specificity in S-nitrosylation: a short-range mechanism for NO signaling? *Antioxid Redox Signal* **19**, 1220-1235, doi:10.1089/ars.2012.5066 (2013).

23 Gould, N., Doulias, P. T., Tenopoulou, M., Raju, K. & Ischiropoulos, H. Regulation of protein function and signaling by reversible cysteine S-nitrosylation. *J Biol Chem* **288**, 26473-26479, doi:10.1074/jbc.R113.460261 (2013).

24 Sharma, K. & Kass, D. A. Heart failure with preserved ejection fraction: mechanisms, clinical features, and therapies. *Circ Res* **115**, 79-96, doi:10.1161/CIRCRESAHA.115.302922 (2014).

25 Ter Maaten, J. M. *et al.* Connecting heart failure with preserved ejection fraction and renal dysfunction: the role of endothelial dysfunction and inflammation. *Eur J Heart Fail* **18**, 588-598, doi:10.1002/ejhf.497 (2016).

26 Chan, M. M. *et al.* Growth differentiation factor 15 in heart failure with preserved vs. reduced ejection fraction. *Eur J Heart Fail* **18**, 81-88, doi:10.1002/ejhf.431 (2016).

27 Tsibris, J. C. *et al.* Selective inhibition of protein disulfide isomerase by estrogens. *J Biol Chem* **264**, 13967-13970 (1989).

28 Borlaug, B. A., Koepp, K. E. & Melenovsky, V. Sodium Nitrite Improves Exercise Hemodynamics and Ventricular Performance in Heart Failure With Preserved Ejection Fraction. *J Am Coll Cardiol* **66**, 1672-1682, doi:10.1016/j.jacc.2015.07.067 (2015).

29 Redfield, M. M. *et al.* Isosorbide Mononitrate in Heart Failure with Preserved Ejection Fraction. *N Engl J Med* **373**, 2314-2324, doi:10.1056/NEJMoa1510774 (2015).

30 Zamani, P. *et al.* Isosorbide Dinitrate, With or Without Hydralazine, Does Not Reduce Wave Reflections, Left Ventricular Hypertrophy, or Myocardial Fibrosis in Patients With Heart Failure With Preserved Ejection Fraction. *J Am Heart Assoc* **6**, doi:10.1161/JAHA.116.004262 (2017).

31 Oeser, C. Heart failure: Nitrates reduce activity levels in HFpEF. *Nat Rev Cardiol* **13**, 2, doi:10.1038/nrcardio.2015.176 (2016).

32 Heemskerk, S., Masereeuw, R., Russel, F. G. & Pickkers, P. Selective iNOS inhibition for the treatment of sepsis-induced acute kidney injury. *Nat Rev Nephrol* **5**, 629-640, doi:10.1038/nrneph.2009.155 (2009).

Figure legends

Figure 1

15 weeks of combination of HFD and L-NAME treatment in mice recapitulates the systemic and cardiovascular alterations of clinical HFpEF.

a, Experimental design. C57BL/6 mice were exposed to the different dietary regimens (blu filled triangle) and followed up to 15 weeks. Echocardiography (Echo), blood pressure measurements (BP), intraperitoneal glucose tolerance test (ipGTT), exercise exhaustion test, pulse wave velocity measurements (PWV), coronary flow reserve measurements (CFR), adult mouse ventricular myocytes (AMVMs) isolation and tissue harvesting were performed at the indicated time points (empty triangles). **b**, Representative left ventricular (LV) M-Mode echocardiographic tracings from different experimental groups. **c**, LV % ejection fraction of different experimental mice (n=15/group). **d**, Global longitudinal strain (GLS) assessment in mouse hearts from different experimental groups (n=8/group). **e**, Representative pulse wave Doppler (top) and tissue Doppler (bottom) tracings from different experimental groups. **f**, E/A ratio of different experimental mice (n=15/group). **g**, E/E' ratio of different experimental mice (n=15/group). **h**, Running distance during exercise exhaustion test in different experimental group of mice (n=8/group). **i**, Heart weight to tibia length ratio (HW/TL) in different experimental group of mice (n=15/group). **j**, Ratio between lung weight (LW) immediately after mouse euthanasia (wet) and after 48h at 65°C (dry) in different experimental group of mice (n=15/group). Box-and-whisker plots show the median, the first and third quartiles, and the minimum and maximum values. Bar graphs show mean ± s.e.m. In d *$p<0.05$, 1-way ANOVA plus Sidak's multiple comparisons test. In f,g,h,i,j **$p<0.001$ and ****$p<0.00001$, 1-way ANOVA plus Sidak's multiple comparisons test.

Figure 2

Robust inactivation of Xbp1s in hearts and cardiomyocytes of HFD + L-NAME mice after five weeks of diet and in human hearts HFpEF samples.

a, mRNA levels of unfolded protein response (UPR) markers in hearts of different experimental groups (n=5/group). **b**, mRNA levels of UPR markers in AMVMs of CHOW and HFD + L-NAME mice (n=5/group). **c**, Representative immunoblot images of pIRE1α, GRP94 and GAPDH proteins in AMVMs of CHOW and HFD + L-NAME mice. Arrow indicates the regulated band. Thapsigargin (Thaps) treatment was used in CHOW AMVMs as a positive control to induce UPR. **d**, Bar graphs showing the ratio between pIRE1α and GAPDH protein bands intensity quantification (n=5/group). **e**, Bar graphs showing the ratio between GRP94 and GAPDH protein bands intensity quantification (n=5/group). **f**, mRNA levels of Xbp1s in right ventricle biopsies from HFpEF and HFrEF subjects (n=12-15/group). In a,f **p<0.001 and ***p<0.0001, 1-way ANOVA plus Sidak's multiple comparisons test. In b,d,e **p<0.001, unpaired Student t test. Data represent mean ± s.e.m for a,b,d,e and box-and-whisker plots show the median, the first and third quartiles, and the minimum and maximum values for f.

Figure 3

Cardiomyocyte-specific Xbp1s overexpression ameliorates diastolic dysfunction and heart failure in experimental HFpEF mice.

a, Experimental design. Control (CTR) and XP1s transgenic mice (TG) were exposed to CHOW or HFD+L-NAME combination of diet (green filled triangle). After five weeks, doxycycline (Doxy) was removed from the drinking water to induce the transgene expression for 2 weeks (blue empty triangle). After this time, mice were subjected to functional analysis and tissue harvesting (Echo, BP, exercise test, tissue harvesting – yellow empty triangle). **b**, LV % ejection fraction of different experimental mice over time (n=7/group). **c**, E/A ratio of

different experimental mice over time (n=7/group). **d**, E/E' ratio of different experimental mice over time (n=7/group). **e**, mRNA levels of *nppa* and *nppb* genes in LV of different experimental group of mice at the end of the study (n=5/group). **f**, Running distance during exercise exhaustion test in different experimental group of mice at the end of the study (n=7/group). **g**, Ratio between wet LW and dry LW in different experimental group of mice at the end of the study (n=7/group). **h**, HW/TL in different experimental group of mice at the end of the study (n=7/group). Data represent mean ± s.e.m for b,c,d,e and box-and-whisker plots showing the median, the first and third quartiles, and the minimum and maximum values for f,g,h. **p<0.001 CTR vs. TG and $^{###}$p<0.0001 CHOW vs. HFD + L-NAME, 2-way ANOVA.

Figure 4

Increased iNOS levels and IRE1α protein S-nitrosylation in experimental HFpEF.

a, mRNA levels of eNOS and iNOS in hearts of different experimental groups (n=5/group). **b**, mRNA levels of iNOS in AMVMs of CHOW and HFD + L-NAME mice (n=5/group). **c**, Representative immunoblot image of TMT and GAPDH proteins in LV of CHOW and HFD + L-NAME mice. **d**, Bar graphs showing the ratio between protein bands intensity quantification (n=4/group). **e**, Representative immunoblot images of SNO-IRE1α and IRE1α proteins in total nitrosylated pool of proteins from LV of CHOW and HFD + L-NAME mice. **f**, Bar graphs showing the ratio between protein bands intensity quantification (n=4/group). In a *p<0.05 and **p<0.01, 1-way ANOVA, in b,d,f *p<0.05, unpaired Student t test. Data represent mean ± s.e.m.

FIGURE 1

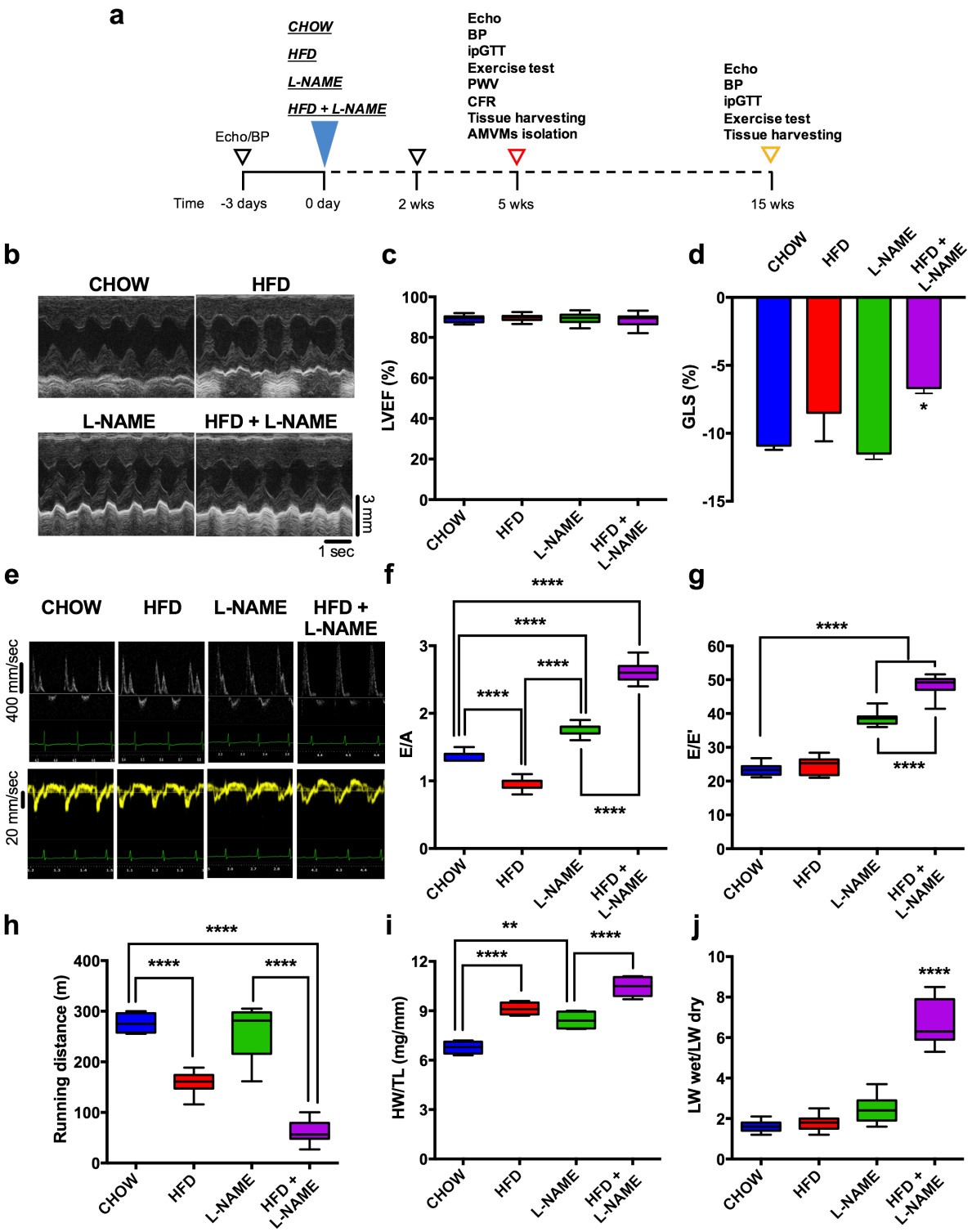
a
CHOW
HFD
L-NAME
HFD + L-NAME
Echo/BP
Echo
BP
ipGTT
Exercise test
PWV
CFR
Tissue harvesting
AMVMs isolation
Echo
BP
ipGTT
Exercise test
Tissue harvesting
Time
-3 days
0 day
2 wks
5 wks
15 wks
b
CHOW
HFD
L-NAME
HFD + L-NAME
3 mm
1 sec
c
LVEF (%)
d
GLS (%)
e
400 mm/sec
20 mm/sec
f
E/A
g
E/E'
h
Running distance (m)
i
HW/TL (mg/mm)
j
LW wet/LW dry

FIGURE 2

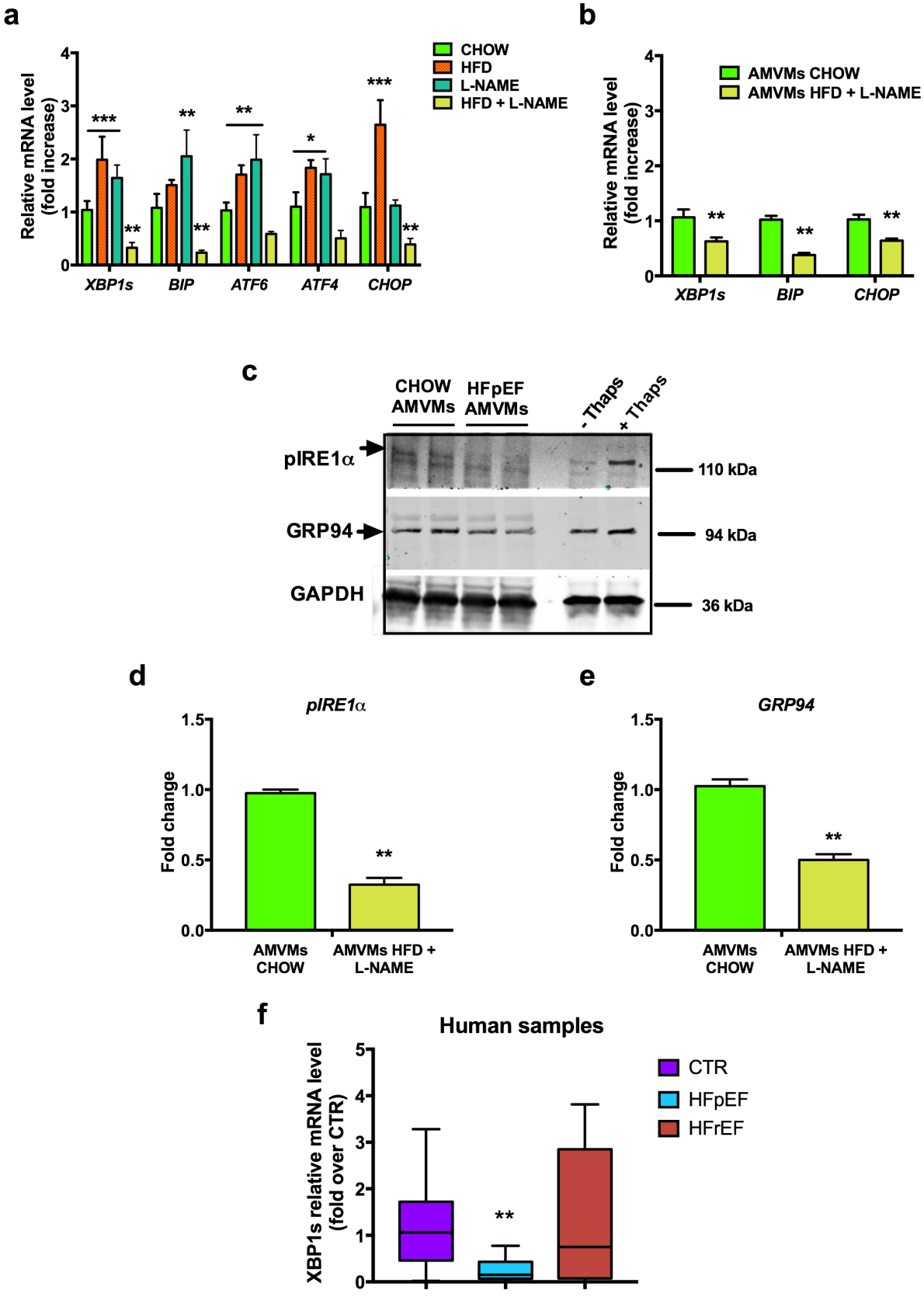
a
Relative mRNA level (fold increase)
CHOW
HFD
L-NAME
HFD + L-NAME
XBP1s
BIP
ATF6
ATF4
CHOP
b
Relative mRNA level (fold increase)
AMVMs CHOW
AMVMs HFD + L-NAME
XBP1s
BIP
CHOP
c
CHOW AMVMs
HFpEF AMVMs
- Thaps
+ Thaps
pIRE1α
GRP94
GAPDH
110 kDa
94 kDa
36 kDa
d
pIRE1α
Fold change
AMVMs CHOW
AMVMs HFD + L-NAME
e
GRP94
Fold change
AMVMs CHOW
AMVMs HFD + L-NAME
f
Human samples
XBP1s relative mRNA level (fold over CTR)
CTR
HFpEF
HFrEF

FIGURE 3

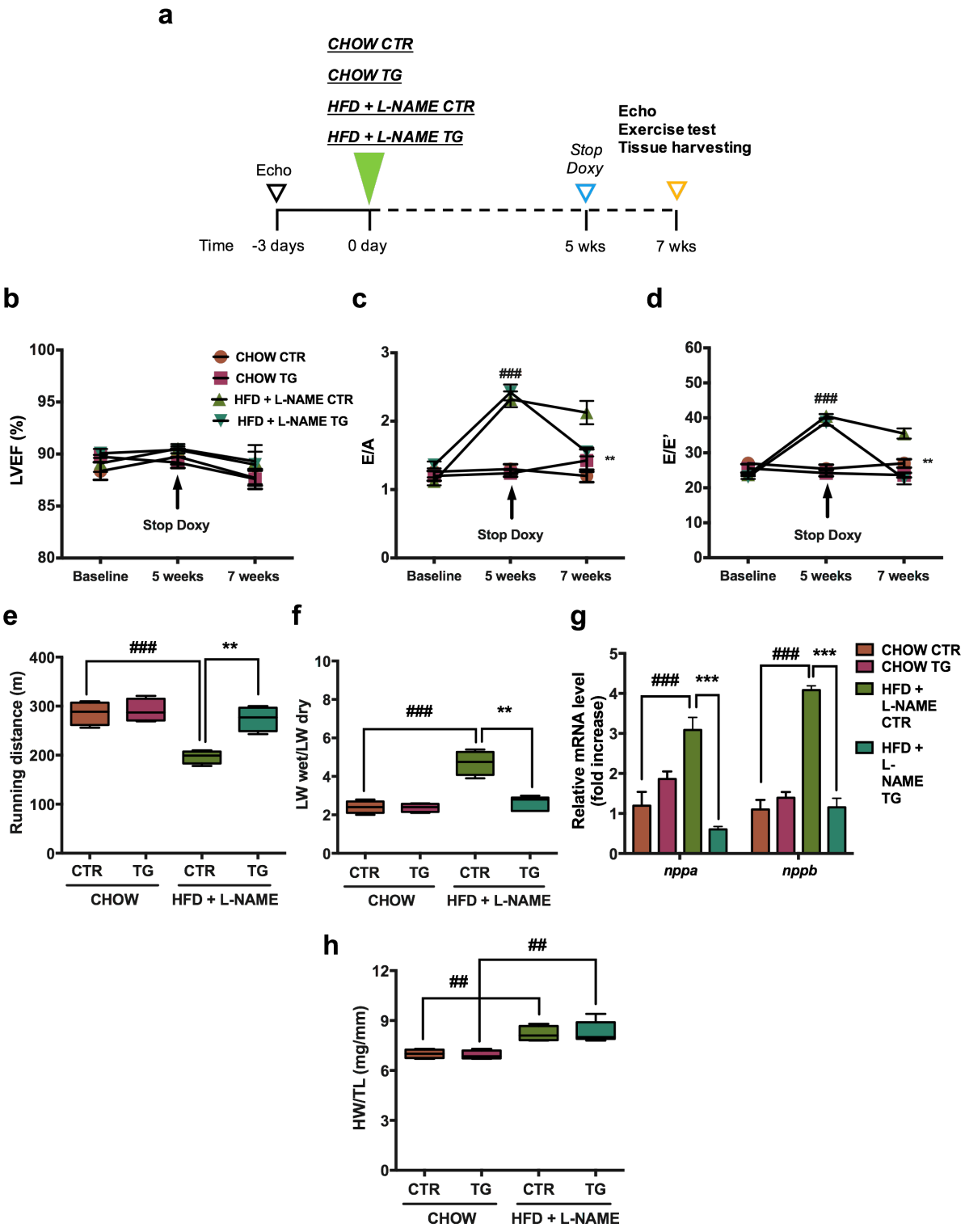
a
CHOW CTR
CHOW TG
HFD + L-NAME CTR
HFD + L-NAME TG
Echo
Stop Doxy
Echo
Exercise test
Tissue harvesting
Time
-3 days
0 day
5 wks
7 wks
b
LVEF (%)
CHOW CTR
CHOW TG
HFD + L-NAME CTR
HFD + L-NAME TG
Stop Doxy
Baseline
5 weeks
7 weeks
c
E/A
###
**
Stop Doxy
Baseline
5 weeks
7 weeks
d
E/E'
###
**
Stop Doxy
Baseline
5 weeks
7 weeks
e
Running distance (m)
###
**
CTR
TG
CTR
TG
CHOW
HFD + L-NAME
f
LW wet/LW dry
###
**
CTR
TG
CTR
TG
CHOW
HFD + L-NAME
g
Relative mRNA level (fold increase)
###
***
###
***
nppa
nppb
CHOW CTR
CHOW TG
HFD + L-NAME CTR
HFD + L-NAME TG
h
HW/TL (mg/mm)
##
##
CTR
TG
CTR
TG
CHOW
HFD + L-NAME

FIGURE 4

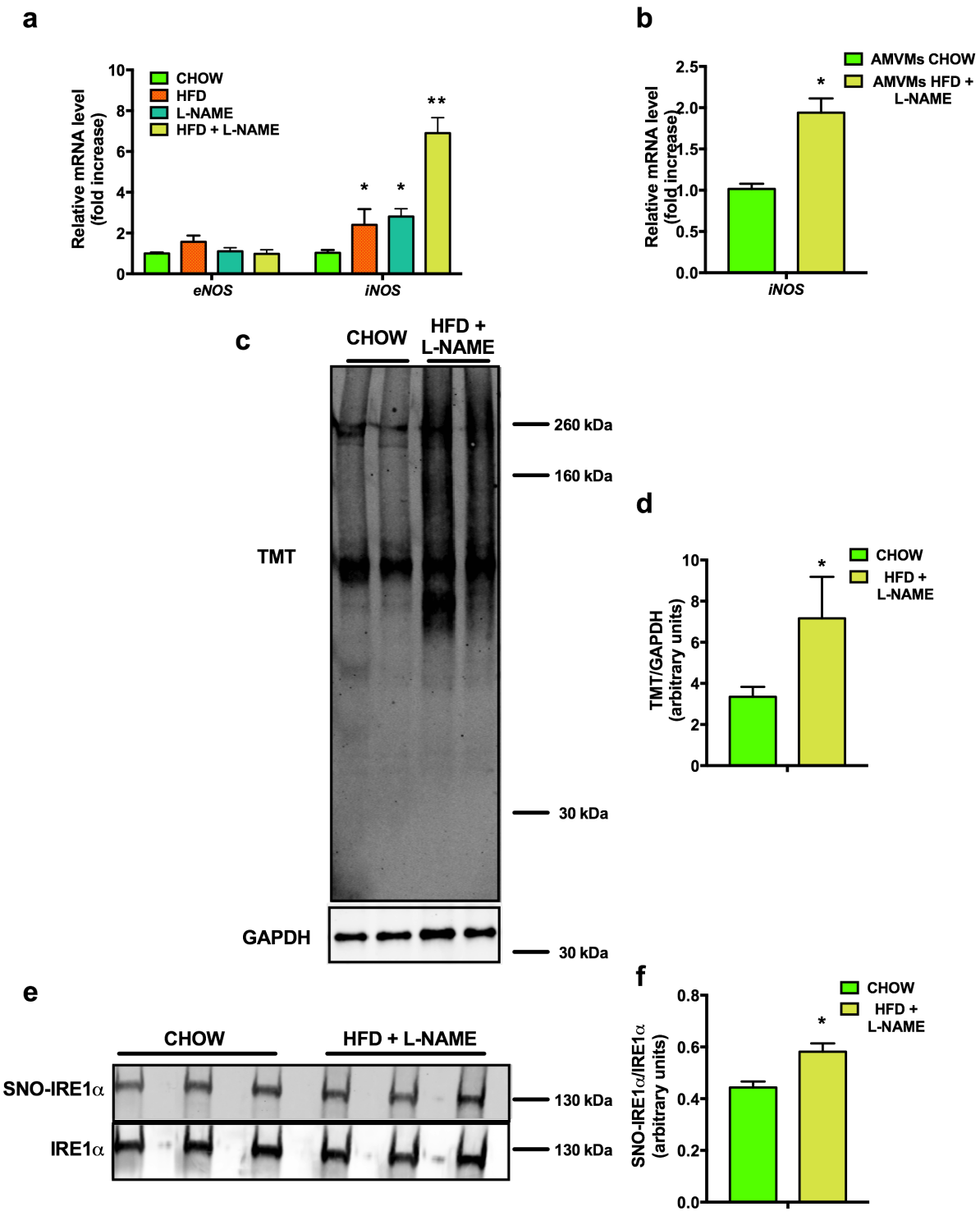
a
Relative mRNA level (fold increase)
CHOW
HFD
L-NAME
HFD + L-NAME
eNOS
iNOS
b
AMVMs CHOW
AMVMs HFD + L-NAME
Relative mRNA level (fold increase)
iNOS
c
CHOW
HFD + L-NAME
260 kDa
160 kDa
TMT
30 kDa
GAPDH
30 kDa
d
CHOW
HFD + L-NAME
TMT/GAPDH (arbitrary units)
e
CHOW
HFD + L-NAME
SNO-IRE1α
130 kDa
IRE1α
130 kDa
f
CHOW
HFD + L-NAME
SNO-IRE1α/IRE1α (arbitrary units)

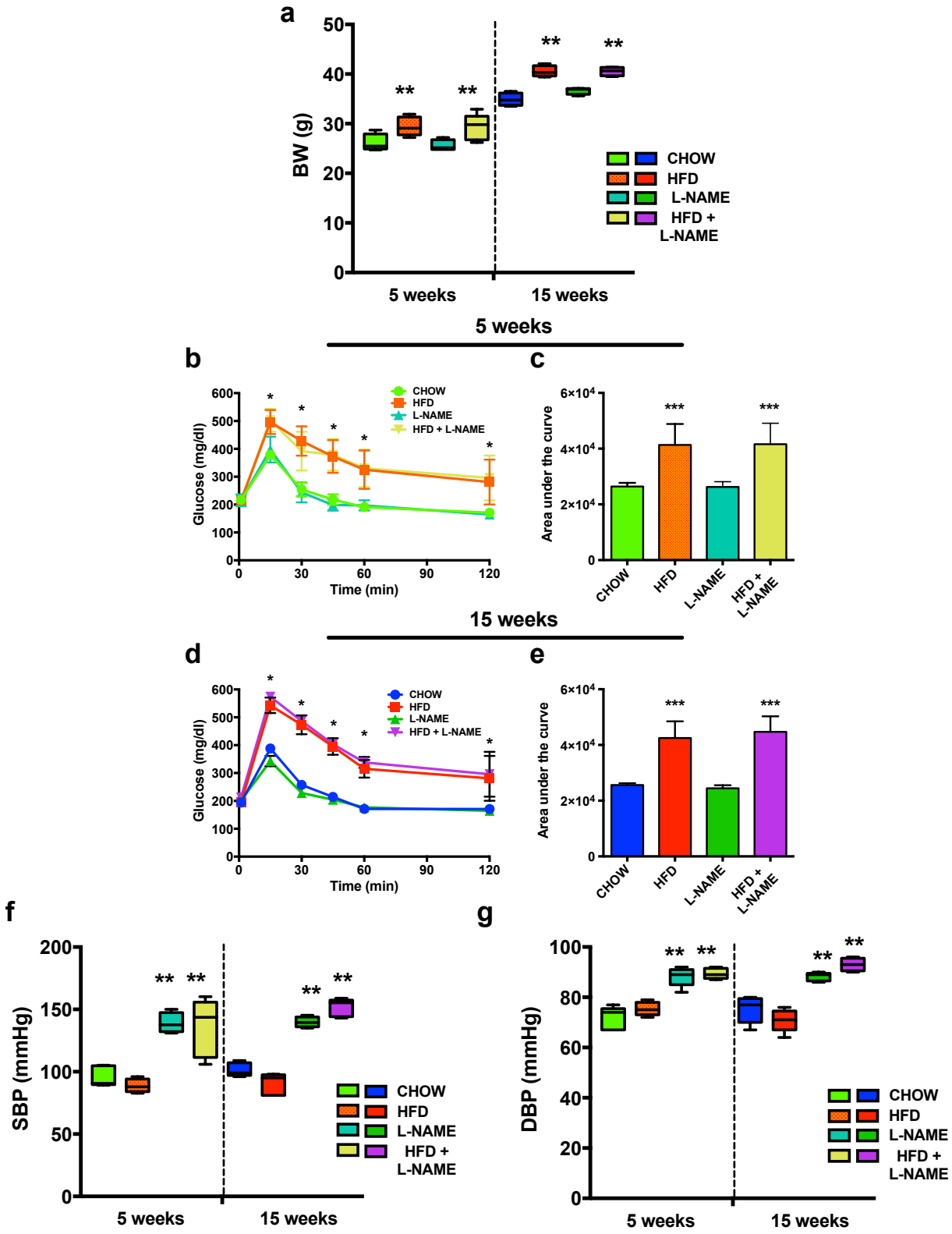

Extended Data Figure 1. Body weight, glucose tolerance test and blood pressure measurements after 5 or 15 weeks of different treatments. **a**, Body weight (BW) in different experimental groups (5 weeks: n=10/group; 15 weeks: n=15/group). **b**, Intraperitoneal glucose tolerance test (ipGTT) in different experimental groups after 5 weeks of treatment (n=10/group). **c**, Bar graphs representing the area under the curve of ipGTT experiment (n=10/group). **d**, ipGTT in different experimental groups after 15 weeks of treatment (n=10/group). **c**, Bar graphs representing the area under the curve of ipGTT experiment (n=10/group). **f**, Systolic blood pressure (SBP) and **g**, diastolic blood pressure (DBP) in different experimental groups at different time points (5 weeks: n=10/group; 15 weeks: n=15/group). Data are presented as box-and-whisker plots showing the median, the first and third quartiles, and the minimum and maximum values, or bar graphs showing mean±s.e.m. *p<0.01, **p<0.001 and ***p<0.0001, 1-way ANOVA plus Sidak's multiple comparisons test or by repeated measurements 1-way ANOVA.

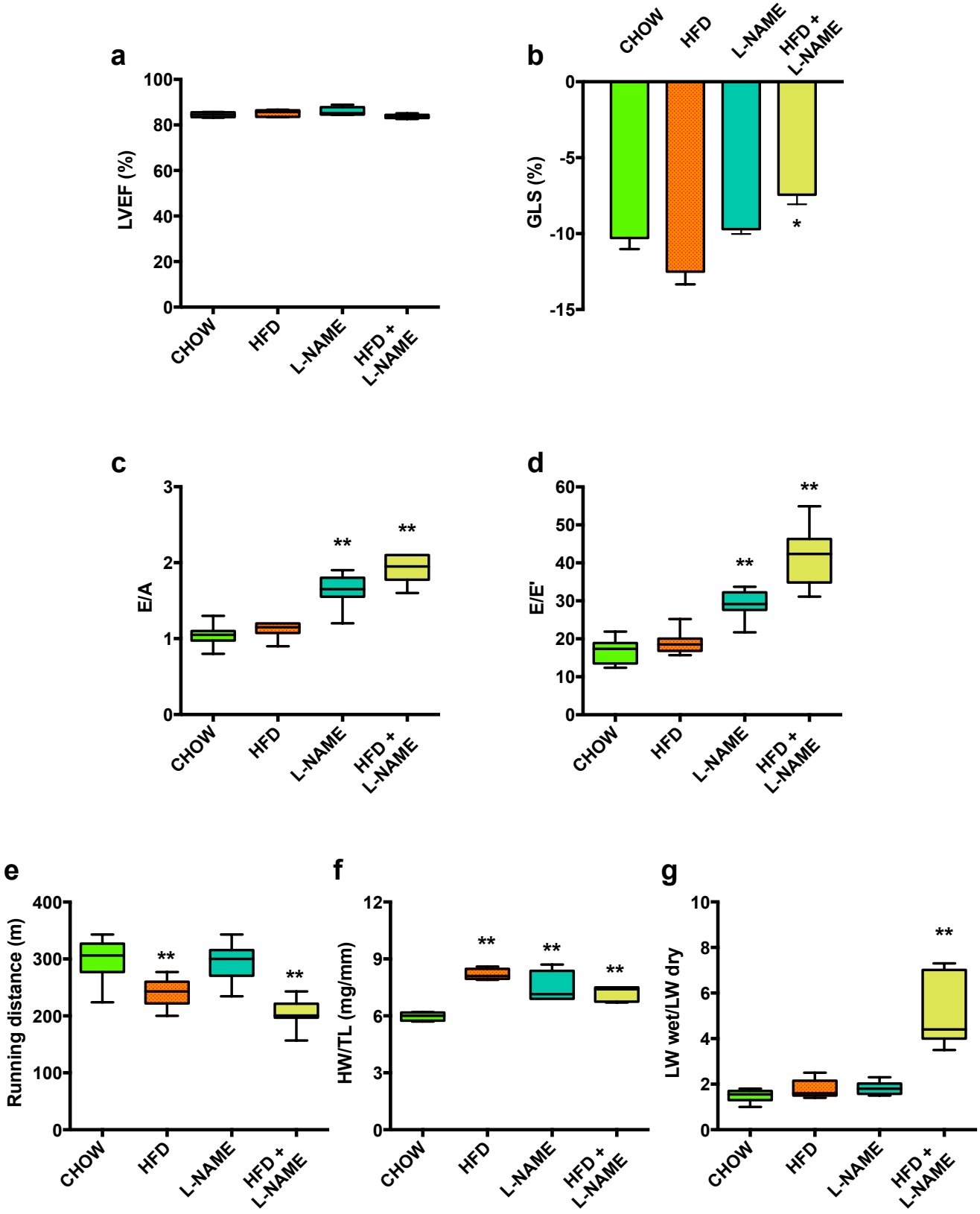

Extended Data Figure 2. Cardiac function characterization and systemic phenotype of mice after 5 weeks of different treatments. **a**, LV % ejection fraction of different experimental groups of mice (n=10/group). **b**, Global longitudinal strain (GLS) assessment in mouse hearts from different experimental groups (n=5/group). **c**, E/A ratio of different experimental mice (n=10/group). **d**, E/E' ratio of different experimental mice (n=10/group). **e**, Running distance during exercise exhaustion test in different experimental group of mice (n=10/group). **f**, Heart weight to tibia length ratio (HW/TL) in different experimental group of mice (n=10/group). **g**, Ratio between lung weight (LW) immediately after mouse euthanasia (wet) and after 48h at 65°C (dry) in different experimental group of mice (n=10/group). Box-and-whisker plots show the median, the first and third quartiles, and the minimum and maximum values. Bar graphs show mean±s.e.m. *p<0.01 and **p<0.001, 1-way ANOVA plus Sidak's multiple comparisons test.

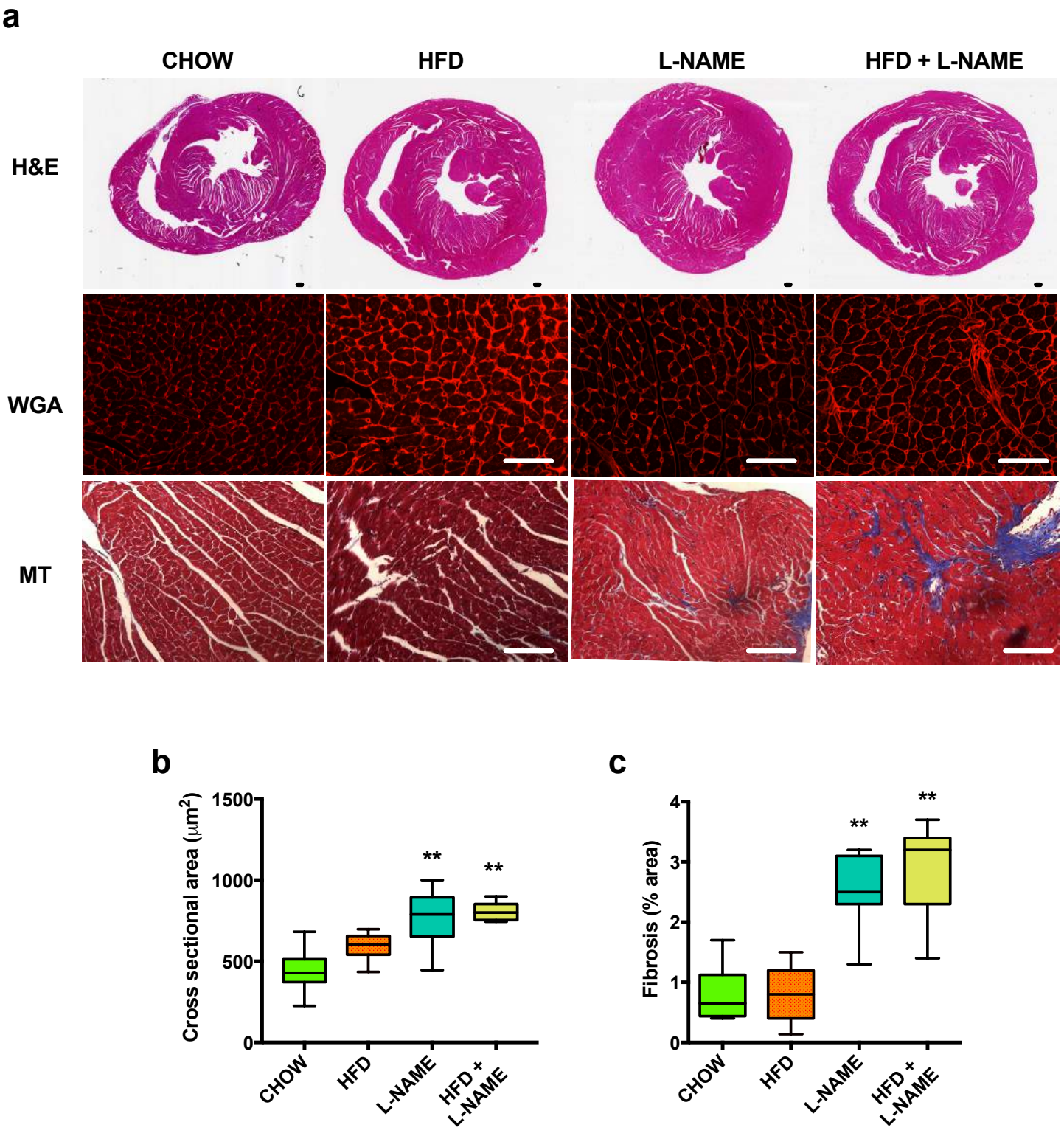

Extended Data Figure 3. Cardiac hypertrophy and fibrosis in 5-week-treated mice. a, Representative images of hematoxylin & eosin (H&E), wheat germ agglutinin (WGA) and Masson's Trichrome staining (MT) of LV of different experimental groups of mice (n=10/group). Scale bar 50 μm. **b**, WGA quantification of mean cross sectional area of 80-10 cardiomyocytes per field (n=10/group; 4 fields/heart). **f**, Fibrosis area % of MT stained cross sections (n=10/group; 4fields/heart). Box-and-whisker plots show the median, the first and third quartiles, and the minimum and maximum values. **p<0.001, 1-way ANOVA plus Sidak's multiple comparisons test.

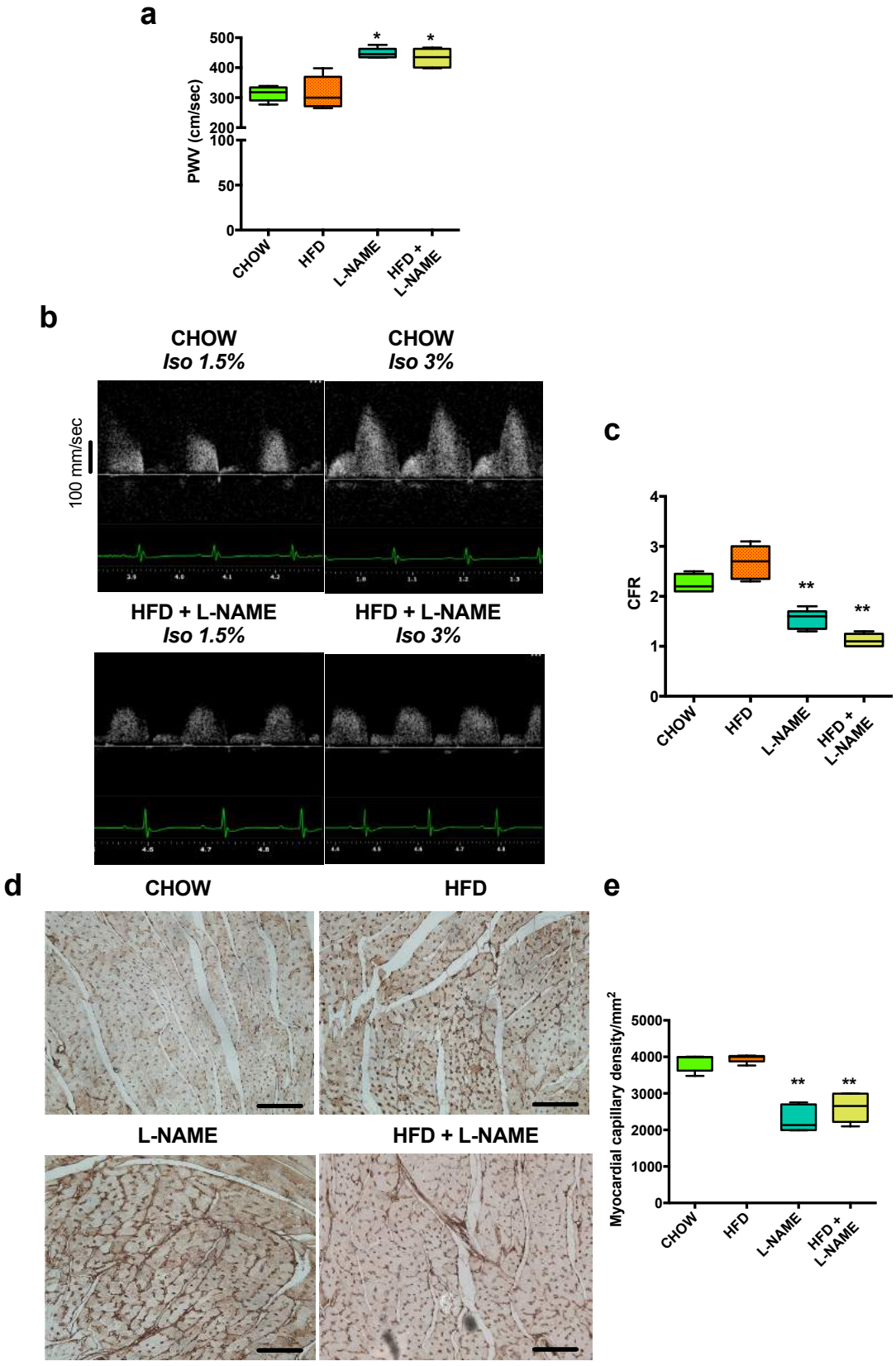

Extended Data Figure 4. Vascular characterization of mice after 5 weeks of different treatments. a, Pulse wave velocity (PWV) in different experimental group of mice (n=5/group). **b**, Representative pulse wave Doppler tracings of coronary flow in CHOW (top panels) and HFpEF (bottom panels) under basal condition (left panels – Iso 1.5%) and after hyperemic stimulus (right panels – Iso 3%). **c**, Coronary flow reserve (CFR) quantification in different experimental group of mice (n=6/group). **d**, Representative images of lectin staining of heart sections in different experimental groups. Capillaries appear brown. Scale bars: 50 µm. **e**, Capillary density in hearts of of different experimental groups (n=6/group). Data are presented as box-and-whisker plots showing the median, the first and third quartiles, and the minimum and maximum values. *p<0.05 and **p<0.001, 1-way ANOVA plus Sidak's multiple comparisons test.

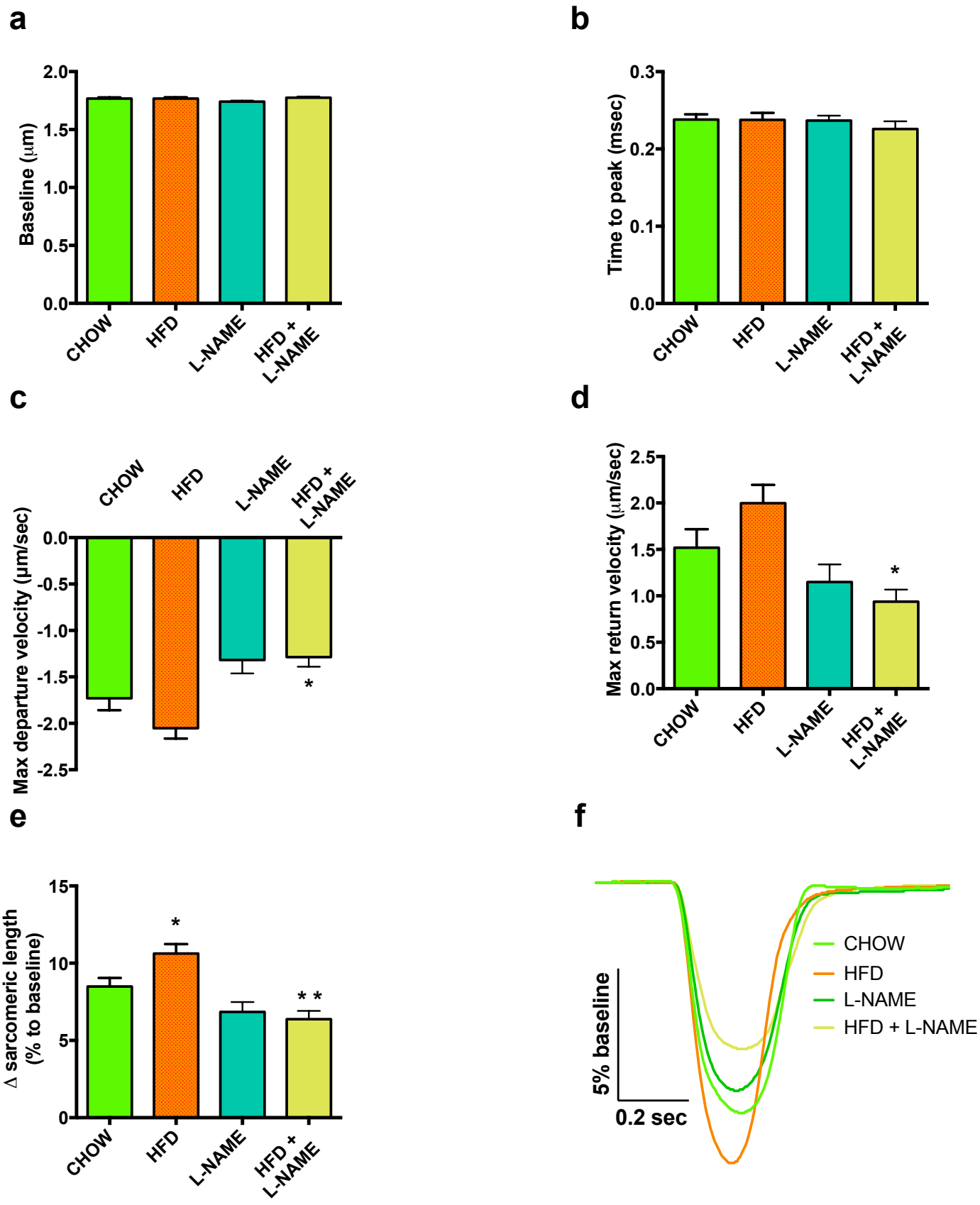

Extended Data Figure 5. Adult mouse ventricular cardiomyocytes contractility in mice after 5 weeks of different treatments. **a**, Baseline sarcomeric length (n=5/group). **b**, Time to peak (n=5/group). **c**, Maximum departure velocity (n=5/group). **d**, Maximum return velocity (n=5/group). **e**, Change in sarcomeric length related to baseline (n=5/group). **f**, Representative tracings of cardiomyocyte contraction/relaxation during pacing (n=5/group). Data are presented as bar graphs showing mean±s.e.m. *p<0.05 and **p<0.001, 1-way ANOVA plus Sidak's multiple comparisons test.

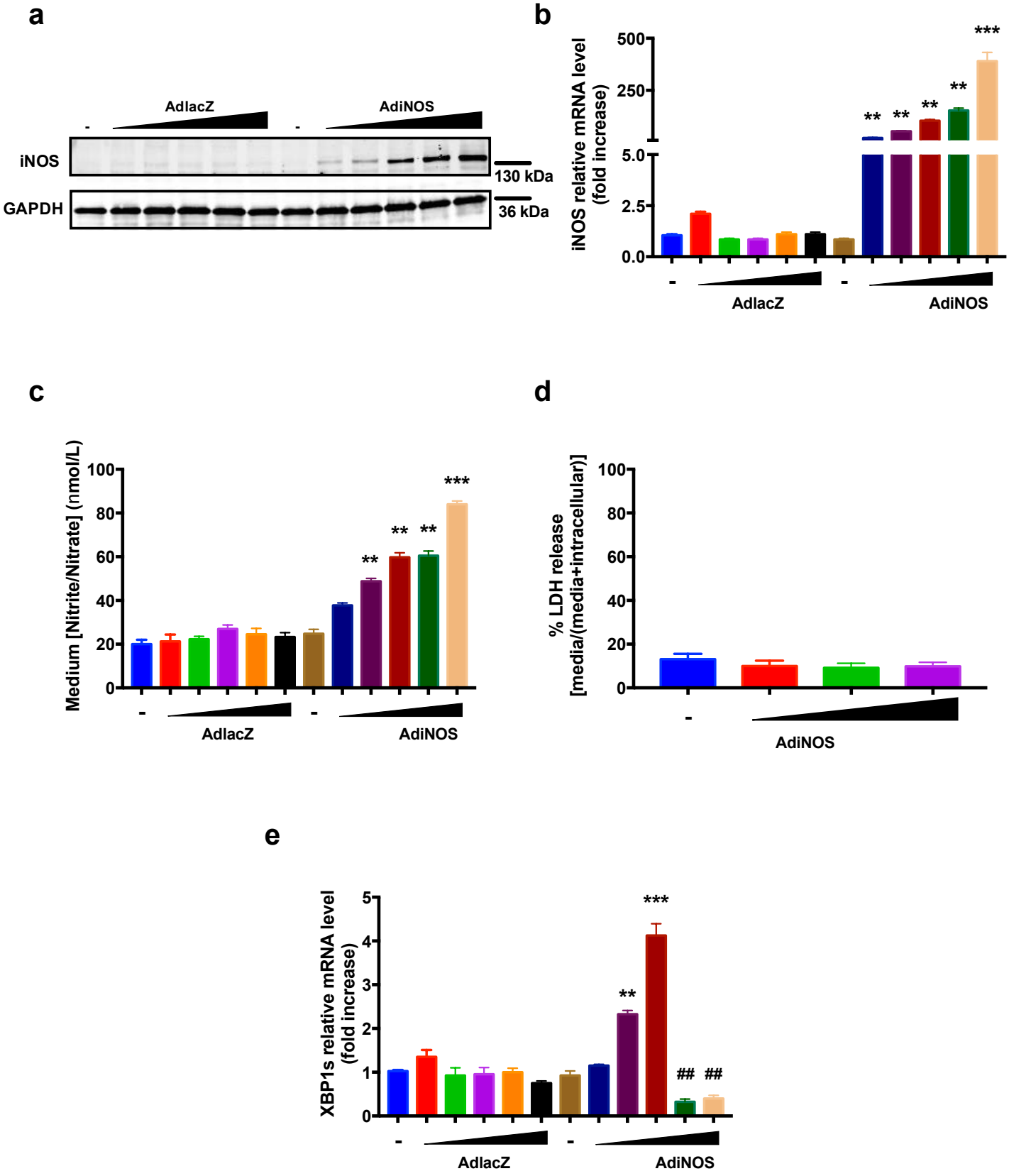

Extended Data Figure 6. iNOS overexpression reduces Xbp1s levels without affecting cardiomyocyte viability. a, Representative images of iNOS and GAPDH immunoblots of NRVMs infected with increasing MOI of AdlacZ and AdiNOS for 24 hours. **b**, iNOS mRNA level of NRVMs transduced with increasing MOI of AdlacZ and AdiNOS for 24 hours (n=5). **c**, Medium Nitrite/Nitrate concentration of NRVMs infected with increasing MOI of AdlacZ and AdiNOS for 24 hours (n=5). **d**, Lactate dehydrogenase (LDH) release in NRVMs transduced with increasing MOI of AdiNOS for 24 hours (n=4). **e**, Xbp1s mRNA level of NRVMs infected with increasing MOI of AdlacZ and AdiNOS for 24 hours (n=5). Data are presented as bar graphs showing mean±s.e.m. **p<0.001, ***p<0.0001, ##p<0.001 1-way ANOVA plus Sidak's multiple comparisons test.

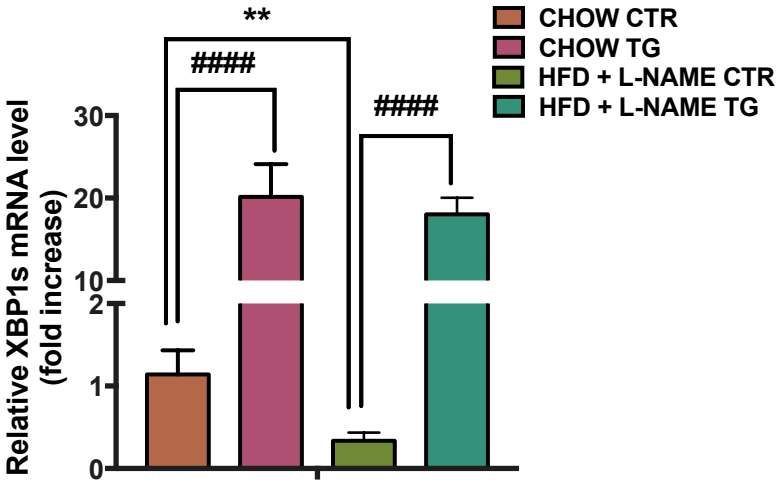

Extended Data Figure 7. XBP1s transgene overexpression in XBP1s TG mice. Xbp1s mRNA level in control (CTR) and XP1s transgenic mice (TG) fed with CHOW or HFD + L-NAME combination of diet for seven weeks. Data are presented as bar graphs showing mean±s.e.m. **p<0.001, ####p<0.00001 1-way ANOVA plus Sidak's multiple comparisons test.